A Dual-Band Millimeter-Wave CMOS Oscillator With Left-Handed Resonator

Alvin Hsing-Ting Yu, *Student Member, IEEE*, Sai-Wang (Rocco) Tam, *Member, IEEE*, Yanghyo Kim, *Member, IEEE*, Eran Socher, *Member, IEEE*, William Hant, *Life Senior Member, IEEE*, Mau-Chung Frank Chang, *Fellow, IEEE*, and Tatsuo Itoh, *Life Fellow, IEEE*

***Abstract*—A new technique using a left-handed (LH) resonator to generate a multiband millimeter-wave carrier signal is proposed in this paper. The LH resonator exhibits nonlinear dispersion characteristic, which enables uneven spacing between resonant frequencies. With N stages of the LH unit cell, there are $N/2+1$ resonant frequencies from the nonlinear dispersion curve. Moreover, the band selection switches are not located in the signal path, which can, therefore, dramatically reduce the size of switches and improve the overall quality factor of the resonator. A dual-band millimeter-wave oscillator in digital 90-nm CMOS technology is implemented to demonstrate this new technique. Using a mode selection switch, the proposed oscillator operates at 21.3 and 55.3 GHz, respectively, with a total power consumption of 14 mW.**

***Index Terms*—CMOS, composite right/left-handed (CRLH), dual band, left-handed (LH), millimeter wave, oscillator, resonator.**

I. Introduction

TRANSMITTING tens of gigabit per second data in multiple bands and dynamic switching across tens of gigahertz are becoming more critical for wireless applications such as those of millimeter industrial, scientific, and medical (ISM) bands at 24 [1] and 60 GHz [2], automotive collision avoidance at 77 GHz [3] and multiband RF-interconnects up to several hundreds of gigahertz [4], [5]. It would be desirable to design a multiband oscillator to cover all or at least part of these frequency bands with fast frequency hopping time, low power consumption, and small silicon area.

Traditionally, implementing a frequency source covering a wide range of frequencies can be done by multiplexing several sources on-chip [6]–[9]. However, in millimeter-wave frequencies, the multiplexer in such a design would require ultra wideband output characteristics, from dc to the highest frequency of interest, which may be achieved using a distributed design [10], at the expense of higher noise, higher power consumption, and larger area.

An alternative approach is to use a single multiband oscillator to cover multiple channels, which was demonstrated to yield superior performance [11]–[13]. In that approach, direct switching of capacitive and inductive elements is used to change the effective *L* and *C* of the voltage-controlled oscillator (VCO) tank. However, in millimeter-wave frequencies, the impedance ratio between OFF and ON states of the CMOS switch is seriously degenerated by parasitic capacitance, and thus seriously degrades the overall quality factor (Q) of the *LC* tank. An alternative to direct multiplexing was proposed using an additional current source switching in a dual-mode transformer-coupled VCO [14], [15]. In this technique, at the higher frequency mode, the Q of the tank is degraded, which consumes extra power. Recently, a switching multiple tank technique has been presented in [16]. In this technique, the parasitic capacitance of buffers and cross-coupled pairs is not lump into the tanks, and thus it limits to lower frequency application.

At millimeter-wave frequencies, the use of a $\lambda/4$ standing wave resonator with artificial dielectric structure [17] becomes more attractive due to smaller size and lower loss. It also leads to the generation of multiple evenly spaced resonant frequencies. However, the inherent even frequency spacing makes it less practical in design for multiband oscillator.

In this paper, a new technique, a left-handed (LH) resonator is presented to implement a multiband millimeter-wave oscillator, which is capable of generating unevenly spaced resonant frequencies [18]. Under this new technique, the band selection switches are not located in the signal path, which can therefore dramatically reduce the size of switches and improve the overall Q of the resonator. Furthermore, compared to the transformer coupling technique, this new technique only utilizes a single pair of cross-coupled pair as a negative resistor without any additional current consumption.

In order to demonstrate the feasibility of this new concept, a dual-band millimeter-wave oscillator using LH resonator at 21 and 55 GHz is constructed in standard digital 90-nm CMOS process.

This paper is organized as follows. Section II presents the composite right/left-handed (CRLH) material theory and the distinct property of CMOS implementation. The CRLH multiband structure is covered in Section III. Even–odd mode analysis of the specific two unit-cell case is described in Section IV. Sections V and VI present circuit design details and measurement results, respectively. Section VII concludes this paper.

Manuscript received August 09, 2009; revised January 22, 2010. First published March 29, 2010; current version published May 12, 2010. This work was supported by Sony and TAPO.

A. H.-T. Yu, S.-W. Tam, Y. Kim, W. Hant, M.-C. F. Chang, and T. Itoh are with the Electrical Engineering Department, University of California at Los Angeles, Los Angeles, CA 90095 USA (e-mail: htyu@ee.ucla.edu).

E. Socher was with the Electrical Engineering Department, University of California at Los Angeles, Los Angeles, CA 90095 USA. He is now with the School of Electrical Engineering, Tel Aviv University, Tel Aviv 69978, Israel.

Color versions of one or more of the figures in this paper are available online at http://ieeexplore.ieee.org.

Digital Object Identifier 10.1109/TMTT.2010.2042854

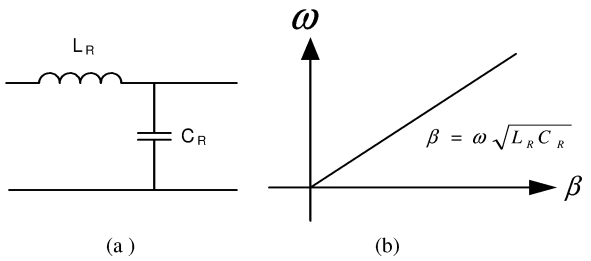

Fig. 1. (a) Equivalent-circuit model of a unit cell. (b) Dispersion diagram of the RH TL.

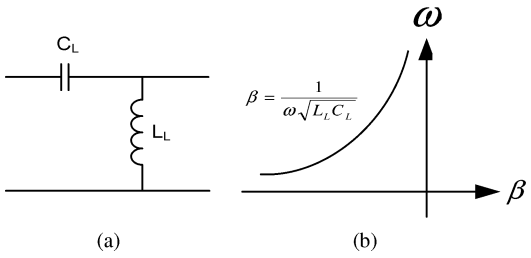

Fig. 2. (a) Equivalent-circuit model of a unit cell. (b) Dispersion diagram of the LH TL.

II. CMOS LH Material

The LH material is usually referred to artificial structure having negative permittivity (ε) and permeability (μ) simultaneously. It has many unique electromagnetic properties such as reversal of Snell's Law and Doppler effect. Recently, many novel microwave devices have been developed based on the LH structure [19].

In contrast to LH structure, most of the ordinary microwave components are right-handed (RH) structures (e.g., transmission line (TL) or stubs) with positive ε and μ. The equivalent-circuit model and dispersion diagram of the RH TL are shown in Fig. 1. The equivalent circuit of the RH TL consists of a series inductor and a shunt capacitor in each unit cell. Since the RH has a linear dispersion characteristic, the phase shift of the RH TL is also linear. Consequently, the RH standing wave resonator can only support evenly spaced resonant frequencies $f_o, 3f_o, \ldots, (2n+1)f_o$, which is the case in a $\lambda/4$ standing wave differential TL resonator.

The equivalent circuit of the LH TL unit cell, on the other hand, consists of a series capacitor and shunt inductor, as shown in Fig. 2(a). As a result, the dispersion characteristic of the LH TL becomes nonlinear, as shown in Fig. 2(b), which is a unique feature compared with the RH TL, making unevenly spaced resonant frequencies possible.

One can easily build an LH TL by integrated several stages of the LH unit cell in Fig. 2(a). However, due to finite parasitic associated with the components in each unit cell, a pure LH TL does not existence in nature. In order to take those undesired parasitic into account, the CRLH model is developed to describe the unique property of this special TL, which is shown in Fig. 3(a). The CRLH TL unit cell [19] consists of a series capacitance C_L and a shunt inductance L_L, as well as a series inductance L_R and a shunt capacitance C_R to account for the parasitic of C_L and L_L, respectively. The dispersion diagram of the CRLH TL is shown in Fig. 3(b), where ω_L and ω_R are the LH and RH cutoff frequencies, and $\omega_{\rm se}$ and $\omega_{\rm sh}$ are the series and shunt resonance frequencies. One can design the desired nonlinear dispersion curve by choosing the four frequencies. Below $\min(\omega_{\rm se}, \omega_{\rm sh})$, C_L and L_L dominate the property of the CRLH TL, where the TL behaves as the LH region. On the contrary, above $\max(\omega_{\rm se}, \omega_{\rm sh})$, L_R and C_R dominate the property of the CRLH TL, where the TL behaves as the RH region. Between the LH and RH regions is a stopband region, where the signal in this frequency is attenuated. In addition, the CRLH TL has a unique feature of supporting *an infinite-wavelength wave* at a finite and nonzero frequency [20].

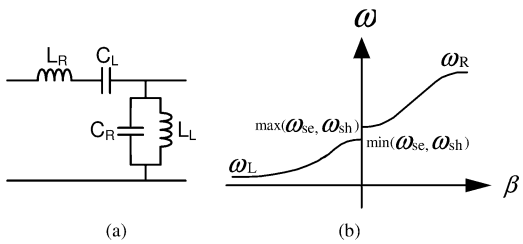

Fig. 3. (a) Equivalent-circuit model of a unit cell. (b) Dispersion diagram of the CRLH TL, where ω_L and ω_R are the LH and RH cutoff frequencies, and $\omega_{\rm se}$ and $\omega_{\rm sh}$ are the series and shunt resonance frequencies.

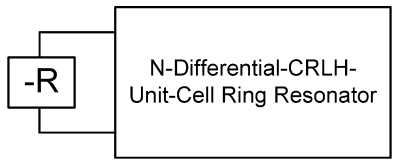

Fig. 4. Conceptual topology of the LH oscillator.

Due to scaling of the CMOS technology, a compact passive structure such as capacitors and inductors are available through a multilayer metal structure. For instance, an on-chip metal–oxide–metal (MOM) capacitor with very small parasitic inductance can have extremely high self-resonant frequency, easily above 100 GHz. Therefore, a CMOS CRLH TL using on-chip MOM capacitors and inductors can be designed to operate in the LH region at millimeter-wave frequencies. On the contrary, in the printed circuit board, due to parasitic of C_L and L_L, the CRLH TL usually has lower series and shunt resonant frequencies $\omega_{\rm se}$ and $\omega_{\rm sh}$, which limits the frequency range of the LH region. In today's CMOS technology, $\omega_{\rm se}$ and $\omega_{\rm sh}$ can possible achieve several hundred gigahertz with careful design, which opens the door for CRLH millimeter-wave and even terahertz research [21].

III. Multiband Resonator Using a CRLH Structure

With an N differential CRLH unit-cell ring resonator and negative resistance with a positive feedback loop, a multiband oscillator can be constructed, as shown in Fig. 4. This N differential CRLH unit-cell ring resonator can be analyzed as two N single-ended CRLH unit-cell ring resonators, one of which is shown in Fig. 5, with differential operation. One of the advantages of the ring topology is that the CRLH unit cell is terminated in itself. The Bloch impedance is well matched, and we can utilize the dispersion curve obtained from an infinite periodic unit cell to analyze the ring resonator.

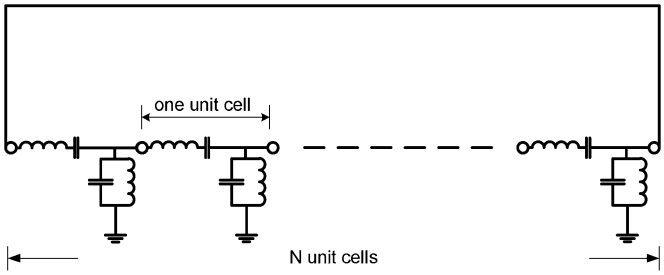

Fig. 5. Single-ended N unit-cell CRLH ring resonator.

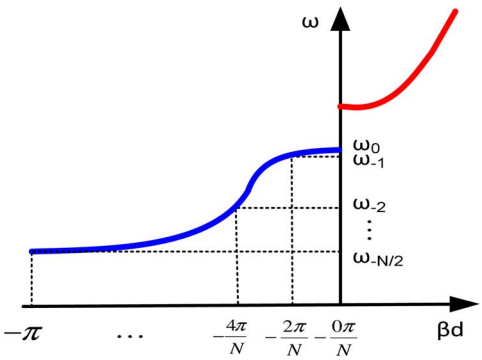

Fig. 6. Dispersion diagram of the N unit-cell CRLH structures with $N/2+1$ resonant frequency.

Two oscillation criteria are [22]

$$\begin{aligned} \mathrm{Re}\{Z\} &> \mathrm{mag}(-R) \\ \mathrm{Im}\{Z\} &= 0 \end{aligned} \tag{1}$$

where Z is the impedance of the tank.

The first condition suggests that the negative resistance compensate the loss from the CRLH structure, the real part of Z of the CRLH structure. The second condition is that the total phase shift of one round trip must be equal to $2n\pi$, where $n = 0, \pm 1, \pm 2, \ldots$. To avoid the oscillator operating in the RH region, we design the series resonance frequency ω_{se} of the CRLH unit cell to be above the unity current gain frequency f_T (120 GHz) of the 90-nm CMOS device. In other words, the oscillator only operates in the LH region. Thus, we get

$$N \times \beta d = 2n\pi, \qquad n = 0, -1, -2 \ldots \tag{2}$$

where βd is the phase shift of one unit cell, and the only negative values of n survive in the LH region operation.

Notice that multiple resonant frequencies can be found from the second oscillation condition in (1) and the dispersion diagram of the CRLH unit cell, as shown in Fig. 6. More precisely, there are $N/2+1$ resonant frequencies in the dispersion curve of the N stages CRLH unit cell. The beauty of this approach is that designers can directly design the spacing of each resonant frequency through a controllable CRLH dispersion curve. Furthermore, the parasitic capacitance of the cross-coupling transistor pairs, output buffers, and L_L is all lumped in the C_R as part of the design. The drawback of such an approach is the loss and area of the LH resonator. However, in millimeter-wave frequencies, the size of the passive device is relatively small, and both the loss and area of the LH resonator can be reduced.

The dispersion diagram of each unit cell can be calculated from the S-parameter. First, we convert the S-parameter to the $ABCD$ matrix. From [23], one can then get

$$\beta d = \mathrm{imag}(\gamma d) = \mathrm{imag}\left[\cosh^{-1}\left(\frac{A+D}{2}\right)\right]. \tag{3}$$

Although the S-parameters depend on the port impedances, the $ABCD$ matrix is unique, and the dispersion curve is unique as well.

By applying the Bloch–Floquet theory to the unit cell in Fig. 5, the resonant frequencies can be found as solution of the dispersion relation of the CRLH TL in [20]

$$\begin{aligned} \beta d &= \frac{-2n\pi}{N} \\ &= \cos^{-1}\left\{1 - \frac{1}{2}\left[\frac{\omega_L^2}{\omega_n^2} + \frac{\omega_n^2}{\omega_R^2} - \left(\frac{\omega_L^2}{\omega_{\mathrm{se}}^2} + \frac{\omega_L^2}{\omega_{\mathrm{sh}}^2}\right)\right]\right\} \end{aligned} \tag{4}$$

where

$$\begin{aligned} \omega_L &= \frac{1}{\sqrt{L_L C_L}} \quad \omega_R = \frac{1}{\sqrt{L_R C_R}} \\ \omega_{\mathrm{sh}} &= \frac{1}{\sqrt{L_L C_R}} \quad \omega_{\mathrm{se}} = \frac{1}{\sqrt{L_R C_L}} \end{aligned}$$

and d is the length of the unit cell. In our case, $\omega_{\mathrm{se}} \gg \omega_{\mathrm{sh}}$, we get

$$\frac{-2n\pi}{N} = \cos^{-1}\left\{1 - \frac{1}{2}\left[\frac{\omega_L^2}{\omega_n^2} - \frac{\omega_L^2}{\omega_{\mathrm{sh}}^2}\right]\right\}. \tag{5}$$

Hence,

$$\frac{1}{\omega_n^2} = \frac{1}{\omega_{\mathrm{sh}}^2} + \frac{2\left[1 - \cos\left(\frac{-2n\pi}{N}\right)\right]}{\omega_L^2}$$

and

$$\omega_n = \frac{1}{\sqrt{L_L\left\{C_R + 2\left[1 - \cos\left(\frac{-2n\pi}{N}\right)\right]C_L\right\}}}. \tag{6}$$

To present the mode selecting switch idea, we choose the two unit-cell ring as an example. A conceptual topology of the dual-band oscillator is shown in Fig. 7, which is composed of a negative resistance and two single-ended two unit-cell rings operated differentially. In this case, $N = 2$, and there are two resonant frequencies $((N/2)+1 = (2/2)+1 = 2)$ corresponding to the $n = 0$ and -1 modes, respectively.

When $n = 0$, we get the higher resonant mode

$$\beta d = 0 \tag{7a}$$

$$\omega_0 = \frac{1}{\sqrt{L_L C_R}} = \omega_{\mathrm{sh}}. \tag{7b}$$

When $n = -1$, we get the lower resonant mode

$$\beta d = -\pi \tag{7c}$$

$$\omega_{-1} = \frac{1}{\sqrt{L_L(C_R + 4C_L)}}. \tag{7d}$$

Notice that at the $n = 0$, node A is 180° out-of-phase with respect to node B. However, at the $n = -1$, node A and node B

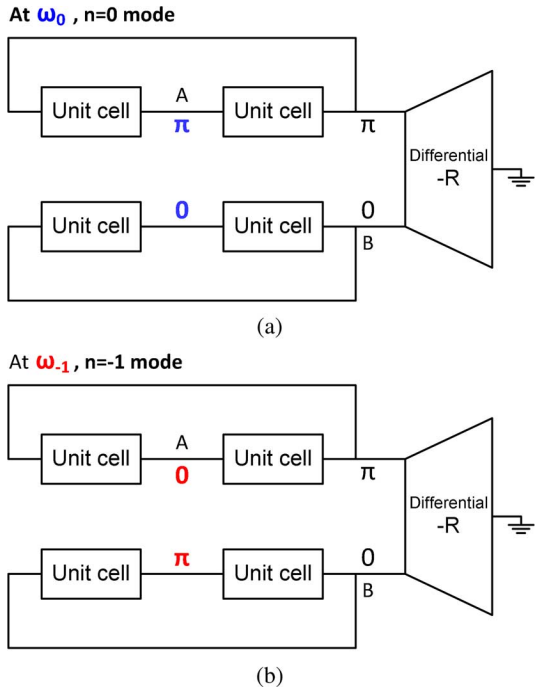

Fig. 7. Conceptual topology of two CRLH unit-cell dual-band oscillator. (a) $n = 0$ mode. (b) $n = -1$ mode.

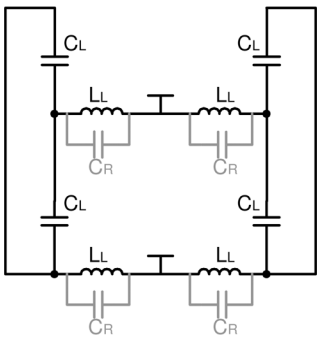

Fig. 8. Schematics of the ring resonator with two differential CRLH unit cells.

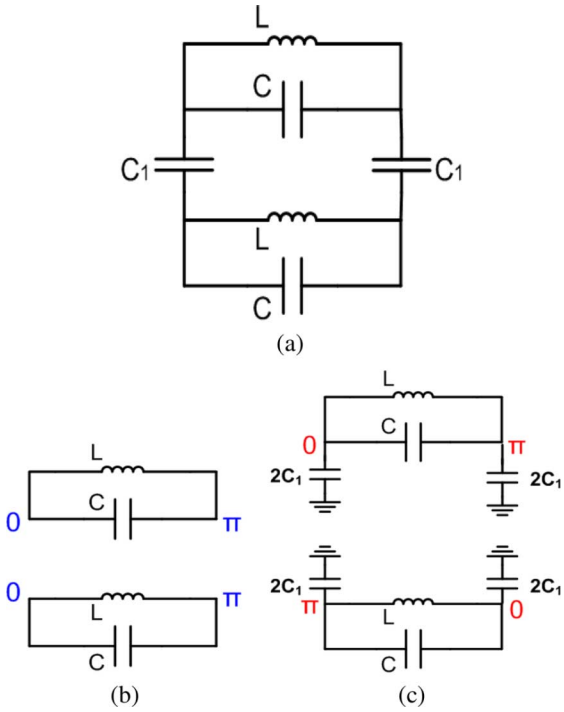

Fig. 9. (a) Simplified CRLH. (b) Even mode operation. (c) Odd mode operation.

are exactly in-phase. Since $\omega_0 > \omega_{-1}$, the tank has higher Q at ω_0, with inductor Q dominating, naturally the oscillator starts to oscillate at ω_0. However, if we add a switch between A and B, which are not located on critical signal paths, we can achieve the mode selection in such a way that the switches enforce the phase shift in one mode and suppress the other mode. That is once we turn on the switch, the $n = 0$ higher resonant mode is suppressed, and the $n = -1$ lower resonant mode is dominant.

IV. Even–Odd Mode Analysis

In the two unit-cell case, we can also describe the dual-band oscillator by even–odd mode analysis. This alternative analysis can verify the oscillating frequency from the CRLH dispersion equation and give us more physical insight. Fig. 8 shows the complete circuit schematic of the two differential CRLH unit-cell ring resonator.

First, we simplify the resonator equivalent circuit as the one in Fig. 9(a) with $L = 2L_L, C = C_R/2$ and $C_1 = 2C_L$. We can then treat this circuit as two LC tanks connected to each other by two capacitors $C_1 s$. Thus, as shown in Fig. 9(b), when the two LC tanks resonate in-phase, the voltage across the capacitor C_1 is zero. On the other hand, when the two tanks resonate at 180° out-of-phase, similar to the Miller effect, the capacitance between two resonator cells is $2C_1$. Based on the equivalent circuit in Fig. 9(c), the resonant frequencies of the even and odd modes are

$$\omega_{\text{even}} = \frac{1}{\sqrt{LC}} = \frac{1}{\sqrt{L_L C_R}}$$

and

$$\omega_{\text{odd}} = \frac{1}{\sqrt{L(C + C1)}} = \frac{1}{\sqrt{L_L(C_R + 4C_L)}}$$

which are exactly the same as ω_0 and ω_{-1}, respectively. We can also directly extend this analysis to estimate the ω_0 and $\omega_{-N/2}$ of the N CRLH unit-cells ring resonator, which are exactly ω_{even} and ω_{odd}.

V. Circuit Design

In order to demonstrate the concept of the multiband oscillator using an LH resonator, a millimeter-wave CMOS oscillator with dual-band operation, 22 and 55 GHz, is implemented. The dual-band oscillator consists of a cross-coupled NMOS pair to act as a negative resistor, two unit cells of an LH structure, and mode selection switches. The dispersion diagram of the unit cell is shown in Fig. 10.

Notice that there is an RH region above the self-resonant frequency of the series capacitor C_L, which is around 100 GHz. Any signal above 100 GHz propagating along the unit cell experiences the RH region instead of the LH region. In addition, there is a bandgap between two regions, LH and RH, which

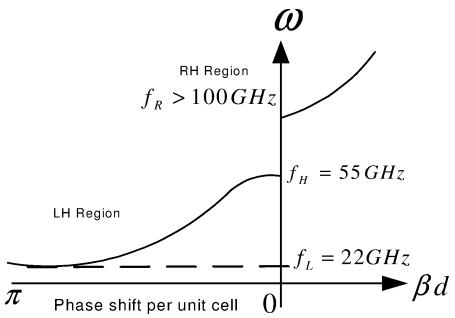

Fig. 10. Two resonant frequencies, 22 and 55 GHz, are shown in the dispersion diagram of the two CRLH unit cells. We use the pure LH region. Notice that there is an RH region above the self-resonant frequency of the series capacitor C_L, which is around 100 GHz. There is also a bandgap in between two regions, RH and LH.

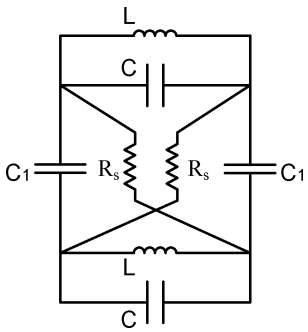

Fig. 11. Model of the mode selection switch with resistor R_s and equivalent circuit of the tank.

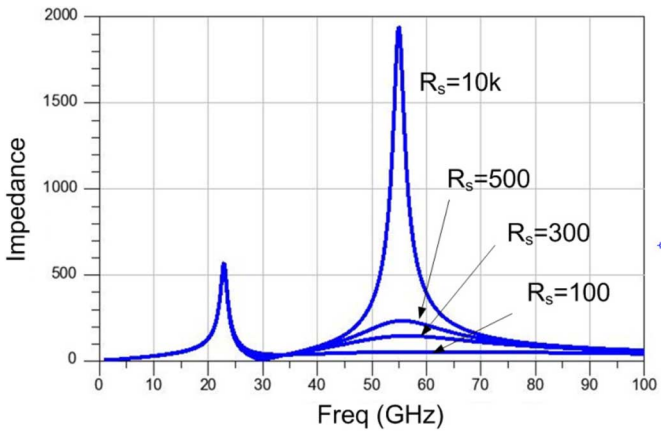

Fig. 12. Tradeoff between the Q of the tank and the size of the mode selection switches as we vary the equivalent resistance R_s of the mode selection switch.

means any signal with frequency content in this bandgap will be attenuated.

In order to study the tradeoff between the Q of the tank and the size of the mode selection switches, we model the selection switch as resistor R_s, and equivalent circuit of the tank is shown in Fig. 11. As we vary the resistance R_s of the switch, we measure the Q of the overall tank through the response of the tank impedance, which is shown in Fig. 12. When $R_s = 10\,\text{k}\Omega$, representing the OFF state of the switch, the impedance at higher resonant mode, 55 GHz, is much higher than that of lower resonant mode, 22 GHz. As a result, the higher resonant mode is dominant in this configuration. Once the value of R_s starts to go

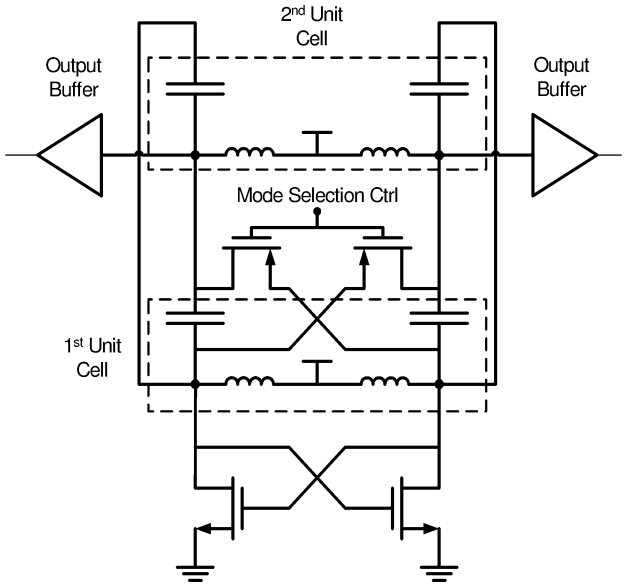

Fig. 13. Schematic of the dual-band millimeter-wave oscillator using LH resonator.

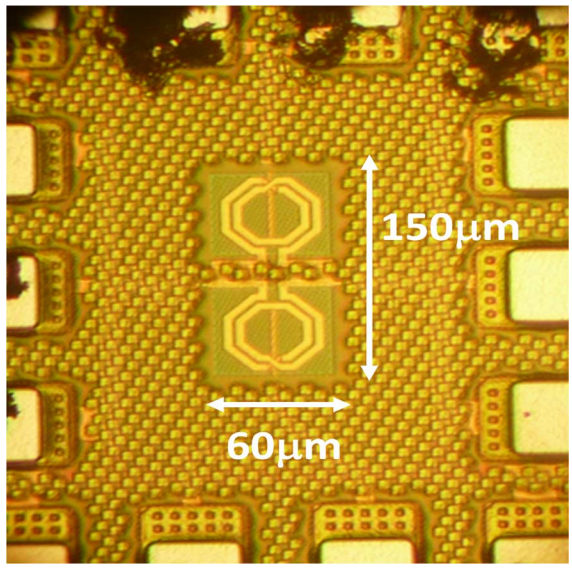

Fig. 14. Chip photograph of the proposed dual-band oscillator.

down, representing the ON state of the switch, the impedance in higher resonant mode get considerably suppressed as well as the Q. On the contrary, the impedance of the lower resonant mode is not affected at all and remains almost unchanged. When the impedance around the higher resonant mode is lower than that of the low resonant mode, the low resonant mode starts to dominate the oscillation. As shown in Fig. 12, even with the on resistance of value as large as 500 Ω, the higher resonant mode is well suppressed. This result suggests that the CMOS switches with small size are enough to perform mode selection, which is the distinguish property of the multiband oscillator with a CRLH resonator.

The full schematic of the proposed dual-band millimeter-wave oscillator is shown in Fig. 13. When the PMOS mode selection switches are on, due to the differential mode op-

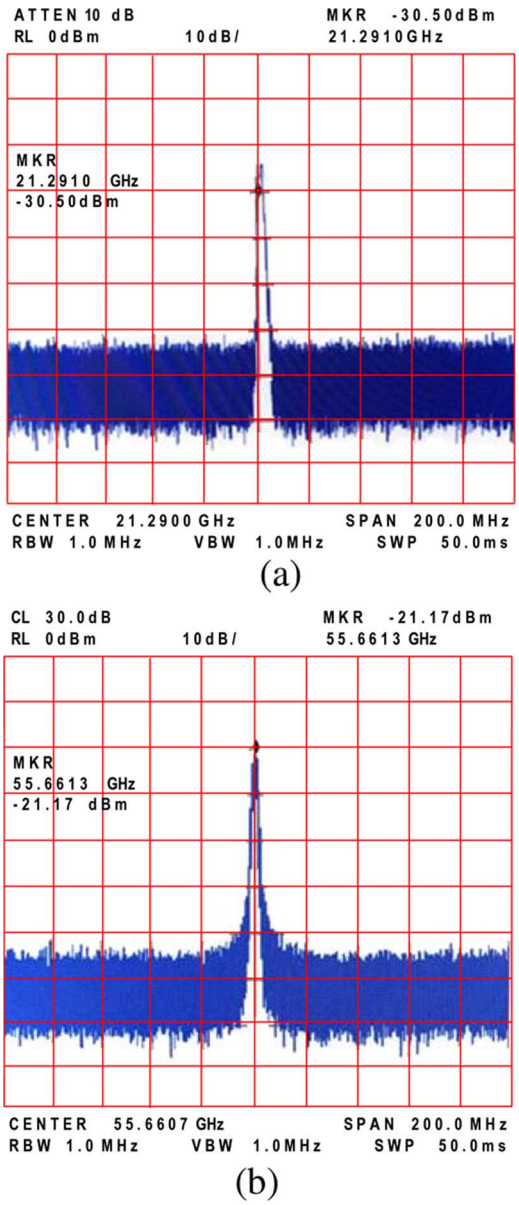

Fig. 15. (a) When the mode selection switches are on, the output frequency is 21.3 GHz. (b) When the mode selection switches are off, the output frequency is 55.6 GHz.

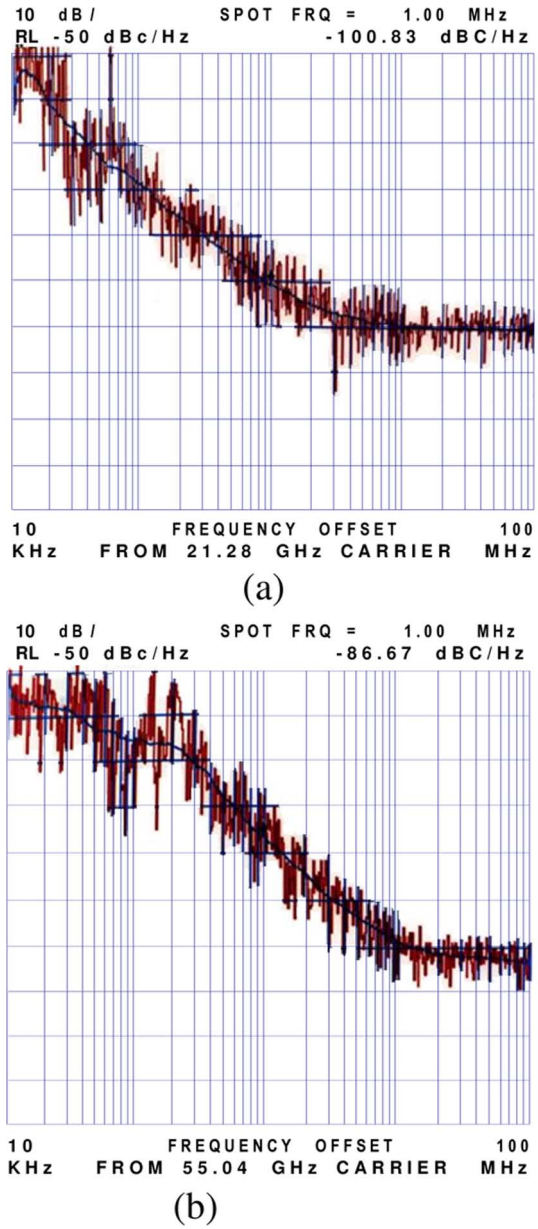

Fig. 16. (a) When the mode selection switches are on, the phase noise at 1-MHz offset is -100.8 dBC/Hz. (b) When the mode selection switches are off, the phase noise at 1 MHz offset is -86.7 dBC/Hz.

eration, the phase shift across the first unit cell is forced to be π. In the beginning of the oscillation, both oscillation mode ω_0 and ω_{-1} are starting at the same time from the thermal noise level. Since the phase between two unit cell is set to be π during the switches are on, the power of ω_{-1} is growing faster and faster and driving the cross-coupled pair to saturation. Eventually, it suppresses the signal in ω_0, and only ω_{-1} survives in the oscillation. On the other hand, when the mode selection switches are off, the phase shift between each unit cell is not limited to any particular value. Therefore, both oscillation modes ω_0 and ω_{-1} compete with each other. In this case, the frequency with lower loss ω_0 dominates the oscillation. In this design, the shunt inductor is 400 pH with Q of 17 at 55 GHz and Q of 9 at 22 GHz, the series capacitor is 50 fF, and the size of mode selection PMOS switch is 10 μm/0.09 μm. The analytic model of the lower resonance mode gives the frequency at 22 GHz and the higher resonance mode gives the frequency at 55 GHz.

VI. Measurement Results

The proposed dual-band oscillator is implemented in an IBM 90-nm standard digital CMOS process. The chip photograph is shown in Fig. 14. The core active area is 150 μm $\times$ 60 μm. When the switch is on, the measured lower resonant frequency ω_{-1} resonates at 21.3 GHz, as shown in Fig. 15(a), with the phase noise of -100 dBc/Hz at 1-MHz offset, as shown in Fig. 16(a). When the switch is off, the measured higher resonant frequency ω_0 resonates at 55.6 GHz, as shown in Fig. 15(b), with the phase noise of -86.7 dBc/Hz at 1-MHz offset, as shown in Fig. 16(b).

TABLE I
MEASUREMENT SUMMARY

Process	IBM 90-nm Digital CMOS Process
Frequency Band	21 GHz and 55 GHz
Frequency Switching Range (GHz)	34.3 GHz
Frequency Switching Range (%)	62% of highest oscillation frequency
Running at 21 GHz Phase Noise @ 1 MHz offset (dBC/Hz)	-100.8
Running at 55 GHz Phase Noise @ 1 MHz offset (dBC/Hz)	-86.7
VCO-Core Power (mW)	14
VCO-Core Area	150 μm × 60 μm

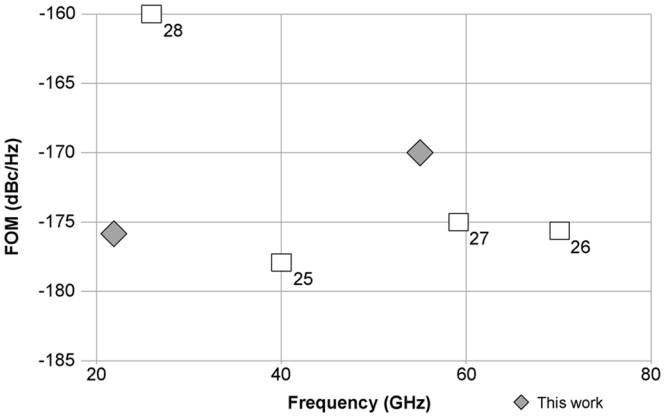

Fig. 17. FOM comparisons of recent published results in millimeter-wave frequencies. $\mathrm{FOM} = L(f_o) - 20\log(f_o/f_{\mathrm{offset}}) + 10\log(P_{\mathrm{dc}}/1\ \mathrm{mW})$.

TABLE II
COMPARISON WITH PREVIOUS WORK

Ref	Tech. CMOS	# of band	f_o (GHz)	P_{DC} (mW)	PN@1M (dBc/Hz)	FOM (dBc/Hz)
This Work	90-nm	2	21	14	-100.8	-175.8
			55		-86.7	-170
[25]	0.18-μm	1	40	27	-100.2	-177.9
[26]	SOI 65-nm	1	70.2	5.4	-106.14 @10M	-175.8
[27]	0.13-μm	1	59	9.8	-89	-175
[28]	0.13-μm	1	26.6	36.5	-96.2@3M	-160

Table I summarizes the measured performance of the proposed dual-band oscillator.

VII. CONCLUSION

A new design technique on arbitrary multiband millimeter-wave oscillator using an LH resonator is proposed in this paper. A dual-band millimeter-wave oscillator in 90-nm CMOS technology has been successfully implemented to demonstrate this new technique. When the mode switch is on, the oscillator operates in lower resonance mode, which is at 21.3 GHz. When the mode switch is off, the oscillator operates in higher resonance mode, which is at 55.3 GHz. These switches are located away from critical signal paths, and therefore, can be made in small size and do not impede the resonator Q. The core area is 150 μm $\times$ 60 μm, and the total power consumption is 14 mW.

In contrast to previous work in the dual-band oscillator [6], [14], [24], the proposed oscillator can switch between the farther band, 21 and 55 GHz, and achieved the largest frequency switching range, 34 GHz. Moreover, this paper has a comparable figure of merit (FOM) with prior work [25]–[28] in the single-band millimeter-wave oscillator, as shown in Table II and Fig. 17.

REFERENCES

[1] X. Guan and A. Hajimiri, "A 24-GHz CMOS front-end," *IEEE J. Solid-State Circuits*, vol. 39, no. 2, pp. 368–373, Feb. 2004.
[2] P. Smulders, "Exploiting the 60 GHz band for local wireless multimedia access: Prospects and future directions," *IEEE Commun. Mag.*, vol. 40, no. 1, pp. 140–147, Jan. 2002.
[3] H. Li, H.-M. Rein, T. Suttorp, and J. Bock, "Fully integrated SiGe VCOs with powerful output buffer for 77-GHz automotive radar systems and applications around 100 GHz," *IEEE J. Solid-State Circuits*, vol. 39, no. 10, pp. 1650–1658, Oct. 2004.
[4] M. F. Chang, J. Cong, A. Kaplan, M. Naik, G. Reinman, E. Socher, and S.-W. Tam, "CMP network-on-chip overlaid with multi-band RF-interconnect," in *Proc. IEEE 14th Int. High Perform. Comput. Arch. Symp.*, Feb. 16–20, 2008, pp. 191–202.
[5] S.-W. Tam, E. Socher, A. Wong, Y. Wang, L. D. Vu, and M.-C. F. Chang, "Simultaneous sub-harmonic injection-locked mm-wave frequency generators for multi-band communications in CMOS," in *Proc. IEEE Radio Freq. Integr. Circuits Symp.*, Jun. 17–Apr. 17, 2008, pp. 131–134.
[6] A. Valdes-Garcia, C. Mishra, F. Bahmani, J. Silva-Martinez, and E. Sanchez-Sinencio, "An 11-band 3–10 GHz receiver in SiGe BiCMOS for multiband OFDM UWB communication," *IEEE J. Solid-State Circuits*, vol. 42, no. 4, pp. 935–948, Apr. 2007.
[7] F. Bohn, H. Wang, A. S. Natarajan, S. Jeon, and A. Hajimiri, "Fully integrated frequency and phase generation for a 6–18 GHz tunable multiband phased-array receiver in CMOS," in *Proc. IEEE Radio Freq. Integr. Circuits Symp.*, Jun. 17–Apr. 17, 2008, pp. 439–442.
[8] O. Werther, M. Cavin, A. Schneider, R. Renninger, B. Liang, L. Bu, Y. Jin, J. Rogers, and J. Marcincavage, "A fully integrated 14 band, 3.1 to 10.6 GHz 0.13 μm SiGe BiCMOS UWB RF transceiver," *IEEE J. Solid-State Circuits*, vol. 43, no. 12, pp. 2829–2843, Dec. 2008.
[9] V. Jain, B. Javid, and P. Heydari, "A BiCMOS dual-band millimeter-wave frequency synthesizer for automotive radars," *IEEE J. Solid-State Circuits*, vol. 44, no. 8, pp. 2100–2113, Aug. 2009.
[10] A. Arbabian and A. M. Niknejad, "A tapered cascaded multi-stage distributed amplifier with 370 GHz GBW in 90 nm CMOS," in *Proc. IEEE Radio Freq. Integr. Circuits Symp.*, June 17, 2008, pp. 57–60.
[11] A. Kral, F. Behbahani, and A. A. Abidi, "RF-CMOS oscillators with switched tuning," in *Proc. IEEE Custom Integr. Circuits Conf.*, May 11–14, 1998, pp. 555–558.
[12] Z. Li and K. K. O, "A low-phase-noise and low-power multiband CMOS voltage-controlled oscillator," *IEEE J. Solid-State Circuits*, vol. 40, no. 6, pp. 1296–1302, Jun. 2005.
[13] M. Tiebout, "A CMOS fully integrated 1 GHz and 2 GHz dual band VCO with a voltage controlled inductor," in *Proc. 28th Eur. Solid-State Circuits Conf.*, Sep. 24–26, 2002, pp. 799–802.
[14] B. Catli and M. M. Hella, "A dual band, wide tuning range CMOS voltage controlled oscillator for multi-band radio," in *Proc. IEEE Radio Freq. Integr. Circuits Symp.*, Jun. 3–5, 2007, pp. 595–598.
[15] A. Bevilacqua, F. P. Pavan, C. Sandner, A. Gerosa, and A. Neviani, "A 3.4–7 GHz transformer-based dual-mode wideband VCO," in *Proc. 32nd Eur. Solid-State Circuits Conf.*, Sep. 2006, pp. 440–443.
[16] A. Goel and H. Hashemi, "Frequency switching in dual-resonance oscillators," *IEEE J. Solid-State Circuits*, vol. 42, no. 3, pp. 571–582, Mar. 2007.
[17] D. Huang, W. Hant, N.-Y. Wang, T. W. Ku, Q. Gu, R. Wong, and M.-C. F. Chang, "A 60 GHz CMOS VCO using on-chip resonator with embedded artificial dielectric for size, loss and noise reduction," in *Proc. IEEE Int. Solid-State Circuits Conf. Tech. Dig.*, Feb. 6–9, 2006, pp. 1218–1227.

[18] S. Tam, H. Yu, Y. Kim, E. Socher, M. C. F. Chang, and T. Itoh, "A dual band mm-wave CMOS oscillator with left-handed resonator," in *Proc. IEEE Radio Freq. Integr. Circuits Symp.*, Jun. 7–9, 2009, pp. 477–480.
[19] A. Lai, T. Itoh, and C. Caloz, "Composite right/left-handed transmission line metamaterials," *IEEE Microw. Mag.*, vol. 5, no. 3, pp. 34–50, Sep. 2004.
[20] A. Sanada, C. Caloz, and T. Itoh, "Novel zeroth-order resonance in composite right/left-handed transmission line resonators," in *Proc. Asia–Pacific Microw. Conf.*, Seoul, Korea, 2003, vol. 3, pp. 1588–1592.
[21] D. Huang, T. R. LaRocca, M.-C. F. Chang, L. Samoska, A. Fung, R. L. Campbell, and M. Andrews, "Terahertz CMOS frequency generator using linear superposition technique," *IEEE J. Solid-State Circuits*, vol. 43, no. 12, pp. 2730–2738, Dec. 2008.
[22] T. Ohira, "Rigorous Q-factor formulation for one- and two-port passive linear networks from an oscillator noise spectrum viewpoint," *IEEE Trans. Circuits Syst. II, Exp. Briefs*, vol. 52, no. 12, pp. 846–850, Dec. 2005.
[23] D. M. Pozar, *Microwave Engineering*, 3rd ed. New York: Wiley, 2005.
[24] J. Borremans, S. Bronckers, P. Wambacq, M. Kuijk, and J. Craninckx, "A single-inductor dual-band VCO in a 0.06 mm^2 5.6 GHz multi-band front-end in 90 nm digital CMOS," in *IEEE Int. Solid-State Circuits Conf. Tech. Dig.*, Feb. 3–7, 2008, pp. 324–616.
[25] J. Chien and L. Lu, "Design of wide-tuning-range millimeter-wave CMOS VCO with a standing-wave architecture," *IEEE J. Solid-State Circuits*, vol. 42, no. 9, pp. 1942–1952, Sep. 2007.
[26] D. D. Kim, J. Kim, J.-O. Plouchart, C. Cho, W. Li, D. Lim, R. Trzcinski, M. Kumar, C. Norris, and D. Ahlgren, "A 70 GHz manufacturable complementary *LC*-VCO with 6.14 GHz tuning range in 65 nm SOI CMOS," in *IEEE Int. Solid-State Circuits Conf. Tech. Dig.*, Feb. 11–15, 2007, pp. 540–620.
[27] C. Cao and K. K. O, "Millimeter-wave voltage-controlled oscillators in 0.13-μm CMOS technology," *IEEE J. Solid-State Circuits*, vol. 41, no. 6, pp. 1297–1304, Jun. 2006.
[28] K. Kwok, J. R. Long, and J. J. Pekarik, "A 23-to-29 GHz differentially tuned varactorless VCO in 0.13 μm CMOS," in *IEEE Int. Solid-State Circuits Conf. Tech. Dig.*, Feb. 11–15, 2007, pp. 194–596.

Alvin Hsing-Ting Yu (S'07) received the B.S. degree and M.S. degrees in physics from the National Taiwan University, Taiwan, in 1998 and 2002, the M.S. degree in electrical engineering from the University of Florida at Gainesville, in 2005, and is currently working toward the Ph.D. degree in electrical engineering at the University of California at Los Angeles (UCLA).

In Fall 2005, he joined the Electrical Engineering Department, UCLA. From April to September 2008 to March 2010, he was with the Broadcom Corporation, as an Internship Radio Frequency Circuit (RF) Design Engineer. In 1994, he represented Taiwan in the 25th International Physics Olympia. His current research interests include the architecture of high-speed transceivers and RF integrated circuits for wireless communications.

Sai-Wang (Rocco) Tam (S'06–M'10) was born in Hong Kong. He received the B.Sc., M.Sc., and Ph.D. degrees in electrical engineering from the University of California at Los Angeles (UCLA), in 2003, 2008, and 2009, respectively.

From 2004 to 2006, he held several summer intern positions with the Microprocessors Mixed-Signal Circuit Group, Intel Corporation, where he was actively involved in 65- and 45-nm complimentary metal–oxide–semiconductor analog mixed-signal circuits design. Since 2008, he has been with WaveConnex Inc., UCLA, where he is a member of the founding team and currently serves as a Principal RF Integrated Circuits Engineer. His current research interests include high-speed mixed-signal circuits, millimeter-wave circuits, high-speed analog/digital, RF-interconnect and network-on-chip.

Dr. Tam was the recipient of the 2008 Best Paper Award presented at the IEEE International Symposium on High-Performance Computer Architecture for his paper entitled "CMP Network-on-chip Overlaid with Multiband RF-Interconnect."

Yanghyo Kim (S'06–M'07) received the B.Sc. degree in electrical engineering from the University of Mississippi, Oxford, in 2007, and is currently working toward the M.Sc. degree in electrical engineering at the University of California at Los Angeles (UCLA).

Since 2008, he joined the High Speed Electronics Laboratory, UCLA, where he is currently with the Electrical Engineering Department, engaged in research on designing low-power high-speed data link for memory application and high-speed analog/digital converter for 60-GHz transceivers.

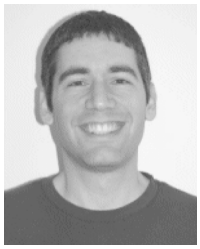

Eran Socher (S"96–M'03) received the B.A. degree (*summa cum laude*) in physics and B.Sc. (*summa cum laude*), M.Sc., and Ph.D. degrees in electrical engineering from Technion—Israel Institute of Technology, Haifa, Israel.

He was engaged in research on complimentary metal–oxide–semiconductor (CMOS)-compatible microelectromechanical systems sensors, and actuators and their readout electronics, especially for uncooled thermal imaging. From 2003 to 2006, he was a Research Engineer with the Israel Defense Forces and an Adjunct Lecturer with Technion and Bar-Ilan University. From 2006 to 2008, he was a Visiting Researcher with the High Speed Electronics Laboratory and a Visiting Assistant Professor with the Department of Electrical Engineering, University of California at Los Angeles (UCLA). Since October 2008, he has been a Senior Lecturer with the School of Electrical Engineering, Tel Aviv University, Tel Aviv, Israel. He has authored or coauthored over 30 journal and conference papers. His current research interests include RF and millimeter-wave CMOS circuit design for high-data rate communication, sensing, and imaging.

Dr. Socher was the recipient of several teaching and research awards and scholarships.

William Hant (S'56–M'57–SM'79–LSM'97) received the B.S. degree from the University of California at Berkeley, the M.S. degree from Stanford University, Stanford, CA, and the Ph.D. degree from the University of California at Los angeles (UCLA), all in electrical engineering.

He possesses over 40 years of diverse research and development experience in applied electromagnetics, measurement technology, and electron device characterization. He was a Principal Engineer with Northrop Grumman, where he was engaged in research on conception and development of special electromagnetic probes to measure impedances of treated surfaces on B-2 aircrafts. He was also involved in the development of millimeter-wave devices, high-speed integrated circuits and in the conception and design of a family of high-voltage large-area filamentary electron guns to stabilize high-energy CO lasers. He was a Project Engineer with Hughes involved with programs to develop coupled-cavity traveling wave tubes and to enhance tube efficiency. He is currently a Visiting Scholar with UCLA, where he is involved in the investigation of how device techniques from other disciplines are adaptable to RF complimentary metal–oxide–semiconductor (CMOS) circuits. An example has been the successful adaptation of artificial dielectrics from antenna theory to the implementation of digitally controlled artificial dielectrics in CMOS circuits.

Mau-Chung Frank Chang (F'96) is currently the Wintek Chair and Distinguished Professor of Electrical Engineering and the Director of the High Speed Electronics Laboratory with the University of California at Los Angeles (UCLA). From 1983 to 1997, he was the Assistant Director and Department Manager of the High Speed Electronics Laboratory, Rockwell Science Center, Thousand Oaks, CA, where he successfully developed and transferred AlGaAs/GaAs heterojunction bipolar transistor (HBT) and BiFET (planar HBT/MESFET) integrated circuit technologies from the research laboratory to the production

line (now Conexant Systems and Skyworks). The HBT/BiFET productions have grown into multibillion dollar businesses and dominated the cell phone power amplifiers and front-end module markets (exceeding one billion units per year). Throughout his career, his research has primarily focused on the development of high-speed semiconductor devices and integrated circuits for RF and mixed-signal communication and sensing system applications. He was the Principal Investigator with Rockwell in leading the Defense Advanced Research Projects Agency's ultra-high speed analog-to-digital (ADC)/digital-to-analog (DAC) development for direct conversion transceiver and digital radar receivers systems. He was the inventor of the multiband reconfigurable RF-Interconnects based on frequency-division multiple access and code-division multiple-access algorithms, for chip multiprocessor inter-core communications, and inter-chip CPU-to-memory communications. He also pioneered the development of the world's first multigigabit per second ADC, DAC, and DDS in both GaAs HBTs and Si CMOS technologies; the first 60-GHz radio transceiver front-end based on transformer-folded-cascode (Origami) high-linearity circuit topology; and the low phase-noise CMOS VCO ($\mathrm{FOM} < -200$ dBc/Hz) with a digitally controlled on-chip artificial dielectric. He was also the first to demonstrate CMOS oscillators in the terahertz frequency range (324 GHz). He has authored or coauthored over 270 technical papers and ten book chapters. He authored one book and edited one book. He holds 20 U.S. patents. He was Guest Editor for the *Journal of High-Speed Electronics and Systems* in 1994.

Prof. Chang was an editor of the IEEE TRANSACTIONS ON ELECTRON DEVICES (1999–2001) and was the guest editor for the IEEE JOURNAL OF SOLID-STATE CIRCUITS (1991 and 1992). He was elected to the U.S. National Academy of Engineering in 2008 for the development and commercialization of GaAs power amplifiers and integrated circuits. He was the recipient of the 2006 IEEE David Sarnoff Award for developing and commercializing HBT power amplifiers for modern wireless communication systems. He was also the recipient of the 2008 Pan Wen-Yuan Foundation Award for his fundamental contributions in developing AlGaAs/GaAs HBT. His paper "CMP network-on-chip overlaid with multiband RF-interconnect" was selected for the 2008 Best Paper Award at the IEEE International Symposium on High-Performance Computer Architecture. He was also the recipient of Rockwell's 1992 Leonardo Da Vinci Award (Engineer of the Year), National Chiao-Tung University's 1997 Distinguished Alumnus Award, and the National Tsing-Hua University's 2002 Distinguished Engineering Alumnus Award.

Tatsuo Itoh (S'69–M'69–SM'74–F'82–LF'06) received the Ph.D. degree in electrical engineering from the University of Illinois at Urbana–Champaign, in 1969.

After working for the University of Illinois, SRI, and the University of Kentucky, he joined the faculty of The University of Texas at Austin in 1978, where he became a Professor of electrical engineering in 1981. In September 1983, he was the Hayden Head Centennial Professor of engineering at The University of Texas at Austin. Since January 1991, he has been with the University of California at Los Angeles (UCLA), as a Professor of electrical engineering and the Holder of the TRW Endowed Chair in Microwave and Millimeter Wave Electronics (currently Northrop Grumman Endowed Chair). He has generated 70 Ph.D. students. He has authored or coauthored over 375 journal publications, 775 refereed conference presentations, and 43 books/book chapters in the area of microwaves, millimeter waves, antennas, and numerical electromagnetics.

Prof. Itoh is a member of the Institute of Electronics and Communication Engineers, Japan, and Commissions B and D of the U.S. National Committee/International Union of Radio Science (URSI). He was an editor of the IEEE TRANSACTIONS ON MICROWAVE THEORY AND TECHNIQUES (1983–1985). He was the president of the IEEE Microwave Theory and Techniques Society (IEEE MTT-S) (1990). He was the editor-in-chief of the IEEE MICROWAVE AND GUIDED WAVE LETTERS(1991–1994). He was elected an Honorary Life Member of the IEEE MTT-S in 1994. He was the chairman of Commission D of the International URSI (1993–1996). He has been on advisory boards and committees of numerous organizations. He was a Distinguished Microwave Lecturer on Microwave Applications of Metamaterial Structures of the IEEE MTT-S (2004–2006). He was also elected to a member of the National Academy of Engineering (2003). He was the recipient of a number of awards including the IEEE Third Millennium Medal (2000) and the IEEE MTT-S Distinguished Educator Award (2000).